Chapter 2

Multifunction Quasi-Z Source-Based Multimode Power Processor for Low-Power EVs

2.1 Introduction

This chapter presents a multifunction quasi-Z source-based multimode power processor for low-power electric vehicles (EVs). In its multifunction, the power processor charges the EV from a single-phase AC supply and can drive the low-power 3-phase AC motor with its inherent quasi-Z source inverter (Q-ZSI) capability. Furthermore, in its multimodal property, the power processor from both vehicles is connected for vehicle-to-vehicle energy exchange by restructuring itself. Also, during the multifunction and multimode operation, auxiliary power supplies are generated for the EV cabin.

Conventionally, different sets of converters are required for multifunction and multimode operations, as shown in Fig. 2.1. An AC/DC and DC/DC converter are used for charging the battery from the single-phase AC supply [76], [77], [78], [79], [80], [81], [82], [83]. Further, another set of DC/AC converters is used to drive the AC motor. Along with that, an additional 12 V battery is required for the low-power auxiliary, and high-power auxiliaries are directly connected to the main battery [84], [85], [86]. In addition to this on-board charger, vehicle-to-vehicle charging is highly sought after in the consumer market, offering mobile charging solutions that help alleviate range anxiety. For that, a bi-directional converter is also added along with the other converters. The various converters required for different functionalities increase the cost of EVs, and they operate independently of one another. Therefore, researchers have integrated more of these functions into a single converter. A list of those integrated converters with similar prior work is represented in Table 2. 1.

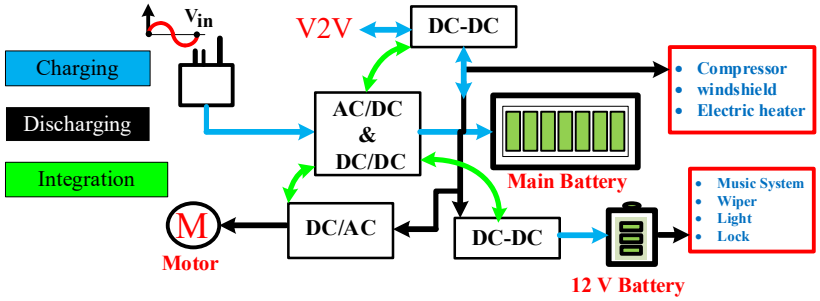

Fig.2. 1 Conventional EV system.

Table 2. 1 Comparative analysis with similar prior work

		[87]	[88]	[89]	[90]	[91]	[65]	Proposed
On-board charger		✓	✓	✓	✓	✓	✓	✓
Motoring operation		×	×	✓	✓	×	×	✓
V2V charging		×	×	×	×	✓	✓	✓
Multioutput		×	✓	×	×	×	×	✓
12 V Auxiliary battery		✓	✓	✓	✓	✓	✓	×
Auxiliary battery charger		✓	×	✓	✓	✓	✓	×
Switches	MOSFETs, Diode	8+12	10+2	6+4	20+0	8	8	10+2
	Changeover Switch	3	2	4	4	0	0	7
	Total	23	14	14	24	8	8	19
Galvanic isolation		✓	×	×	✓	×	×	✓
Total Functions		1	2	2	2	2	2	4

The main contribution of this proposed power processor is as follows:

1. In multifunction operation, three outputs are generated. In single-phase charging, three outputs are generated from the single-phase AC supply, 1st output charges the battery with a constant-current and constant-voltage technique, and 2nd and 3rd outputs power the EV's cabin.
2. Further, in motoring mode, three outputs are generated from the battery. 1st buck-boost AC output is generated by the inherent quasi-Z source property with modified sinusoidal pulse width modulation (M-SPWM) switching, and 2nd and 3rd outputs cater to the power demand of the EV cabin. The changing mode to motoring mode is transferred with the help of seven additional switches, and vice versa for motoring to charging mode.
3. In its multimode property, the V2V charging circuit is structured by four changeover switches for the energy exchange.
4. The multi-output of the proposed power processor in each operating mode replaces the additional requirement of a 12 V battery and charger from the EVs. Further, its power scale can be upgraded according to the demand.

2.2 Operation of the proposed power processor:

The idea of a multifunctional and multimode operation provides single-phase charging, motoring operation, and vehicle-to-vehicle charging. In all these modes of operation, the auxiliary outputs are available to power the EV cabin. The circuit diagram of the proposed power processor is shown in Fig.2. 2. All modes of operation are mutually exclusive, and transitions between modes are carried out at standstill using seven changeover switches.

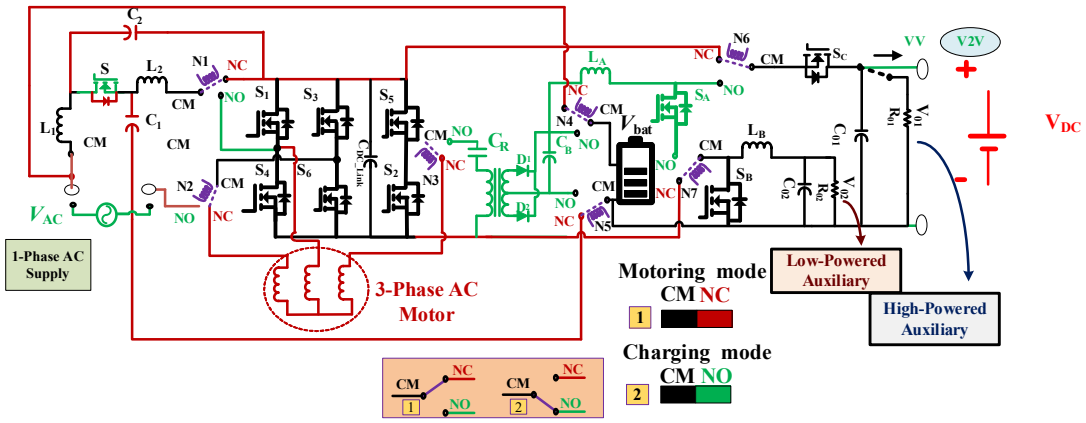

Fig.2. 2 Circuit diagram of the proposed multifunction quasi-Z source-based multimode power processor.

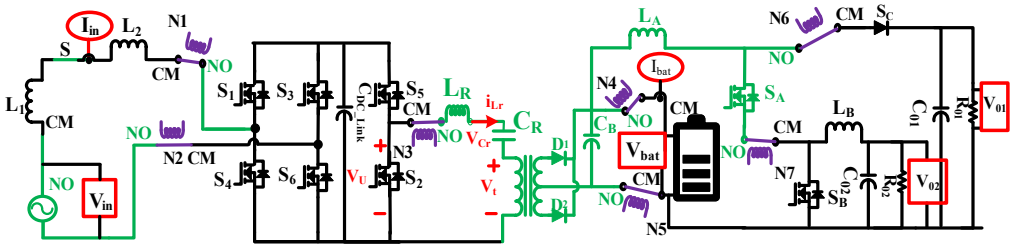

Fig.2. 3 Circuit diagram of the proposed power processor during charging mode.

The changeover switch has three contact points: 1) common contact (CM), 2) normally closed contact (NC), and 3) normally open contact (NO). The charging mode is formed by the CM-NO connection between seven additional switches, along with switch S of the converter, which remains turned ON, as shown in Fig.2. 3 . In propulsion mode, a CM-NC connection is formed between the six additional switches, and switch S is turned OFF, as shown in Fig.2. 4.

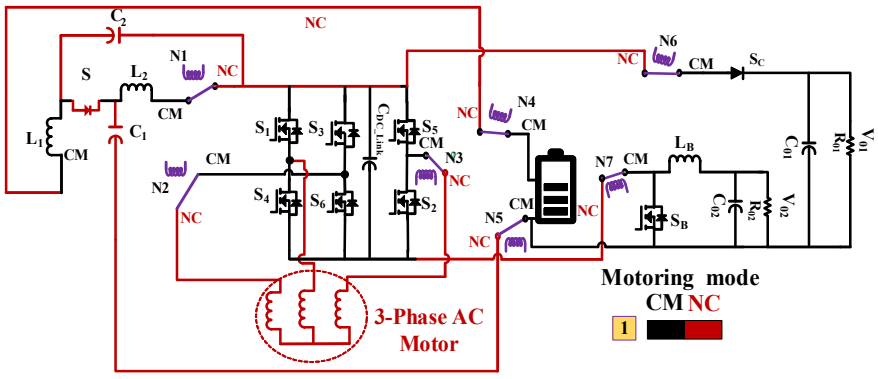

Fig.2. 4 Circuit diagram of the proposed power processor in propulsion mode.

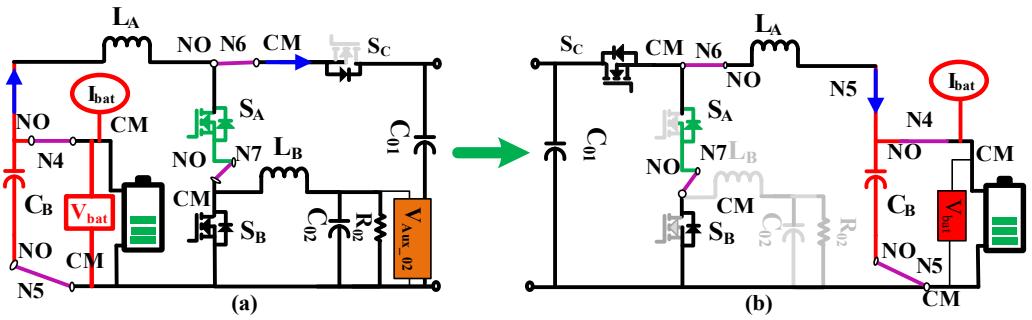

Fig.2. 5 Circuit connection for the V2V charging, a) circuit of the energy supplier vehicle, and (b) circuit of the energy acceptor vehicle.

Furthermore, the V2V circuit is structured with the CM-NO connection established in N4, N5, N6, and N7 changeover switches. For V2V charging, the proposed power converter from both vehicles is directly connected, as shown in Fig.2. 5 .

The operation of the proposed power processor in its multifunction and multimode operation:

2.2.1 Multifunction operation of the proposed power processor

2.2.1.1 Charging operation:

In the charging operation, it maintains the unity power factor at the source terminal and prevents the harmonic, which pollutes the grid. Also, the regulated outputs are generated for the cabin power demand.

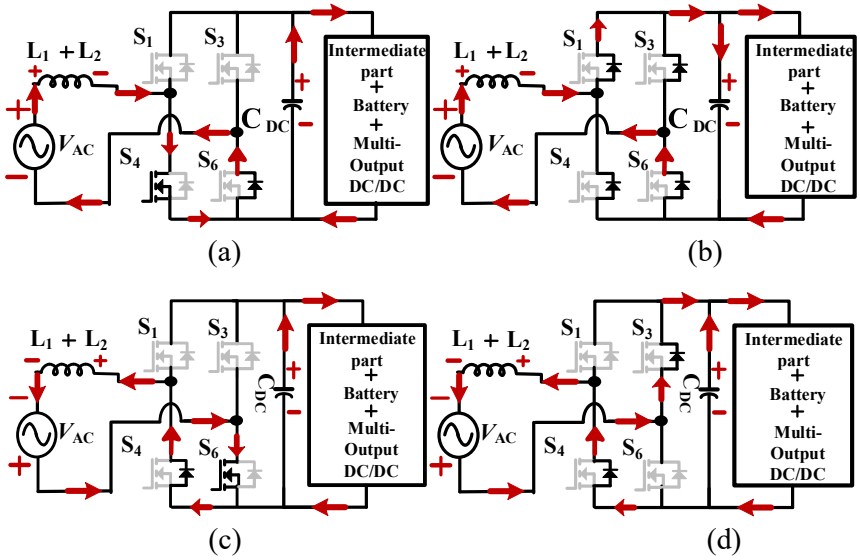

Fig.2. 6 Operation of front-end PFC converter during positive cycle of source voltage, (a) S4-S6 is ON, (b) both switches are OFF, during negative cycle of the source voltage (c) S4-S6 are ON, (d) both switches are OFF.

a) PFC operation of the proposed power processor:

For the charging, a standard household AC power source of 120 V, 50 Hz, is connected at the front end of it. The front end of the proposed power processor consists of source inductance, switches S_1, S_3, S_4, and S_6, and the DC-link capacitance, which maintains the unity PF at the source terminal with a boost DC-link voltage. The source inductance is formed by adding L_1 and L_2 through tuning on the switch S. The operation of the front-end of the proposed power processor can be understood with the help of two modes: 1) the Positive cycle of the supply source, and 2) the Negative cycle of the supply source.

Mode I: - Converter operation during the positive and negative cycles of the single-phase power supply is shown in Fig.2. 6 (a) and (b). During the positive cycle of the power supply, when the switch S_4 is ON, the source inductor is charged by the source voltage, and at the same time, C_{DC} is discharged into the load, as shown in Fig.2. 6(a). When the switch S_4 is OFF, the source voltage and stored energy in the inductor are released into the DC-link capacitor, shown in Fig.2. 6(b). In this way, the DC-link voltage V_{DC} becomes greater than the input V_{AC} voltage in the positive cycle of the source voltage. This pattern remains the same for the whole positive cycle of the supply voltage.

Mode II - During the negative cycle of the supply source, the operation of switch S_4 is replaced by switch S_6, and its operation can be understood in Fig.2. 6(c) and (d).

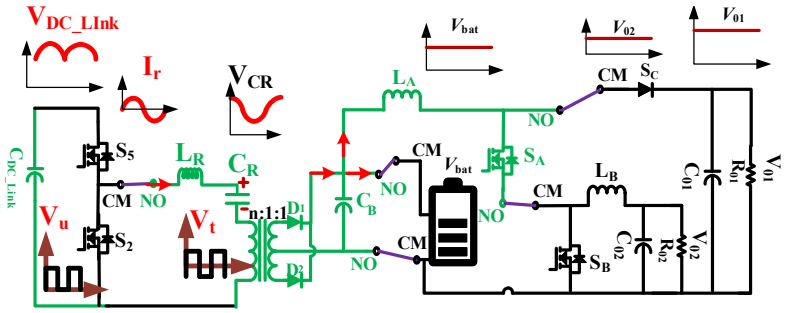

Fig.2. 7 Three DC outputs are generated during the charging mode by the proposed power processor.

b) DC outputs during single-phase charging mode:

The circuit illustrating the three DC outputs generated by the proposed power processor in charging mode is shown in Fig.2. 7. The battery is charged from the intermediate part of the proposed power processor, and dual output power supports the EV cabin. The intermediate part of the proposed power processor (PPP) operates on the principle of series resonance with a fixed duty cycle and provides constant gain with zero voltage switching (ZVS). The series

resonance suppresses the harmonics and interference to a certain extent. The fixed duty cycle with constant gain reduces the control complexity for the DC-DC converter during on-board charging. For the ZVS condition, when the switch is turned ON, the switch current I_{DS} lags the switch voltage $V_{DS,}$ and then the current will pass through the body diode. So, the switching loss is reduced during the turn-on time.

The multioutput of PPP in charging extracts power from the AC source. It generates two more DC outputs along with the battery charging: 1) boost DC (V_{01}), and 2) buck DC (V_{02}). It connects with different orientations in propulsion mode and generates three outputs from the battery.

c) Constant gain of the converter

The normalized output terminal voltage of the PPP for the battery charging can be represented as:

$$V_{bat} = g_{LLC\_n} * \frac{1}{n} * {}^{V_{dc\_link}}/_{2} \tag{2.1}$$

$$g_{LLC\_n} = \left| \frac{L_n * {f_n}^2}{[(L_n+1)*{f_n}^2-1]+j[({f_n}^2-1)*f_n*Q_L*L_n]} \right| \tag{2.2}$$

$$g_{LLC\_n} = 1, at\ f_n = 1$$

Where: normalized gain (g_{LLC_n}), normalized frequency (switching frequency (f_s)/ resonance frequency (f_r)), quality factors (Q_L), and normalized inductance (L_n).

d) Relation between battery and dual output voltages

Steady-state analysis can be explained in three modes: shoot-through, power, and zero-state. In the shoot-through state, S_A and S_B switches are turned ON; in the power state, S_A remains ON and S_B is turned OFF, while in the zero state, both switches S_A and S_B are turned OFF. By applying the flux balance in inductors L_A and L_B, the steady state voltage equation of the boost and buck mode of the multioutput is given as:

$$V_{01} = \frac{V_{bat}}{(1-D_1)} \tag{2.3}$$

$$V_{02} = V_{01} * D_2 \tag{2.4}$$

2.2.1.2 Motoring mode operation:

During propulsion operation, all seven additional switches of the PPP's CM connector are connected to the NC connection, as shown in Fig.2. 4. In this operation, three outputs are generated from the battery with modified sinusoidal pulse width modulation (M-SPWM) switching logic in an inherent Q-ZSI-based structure:

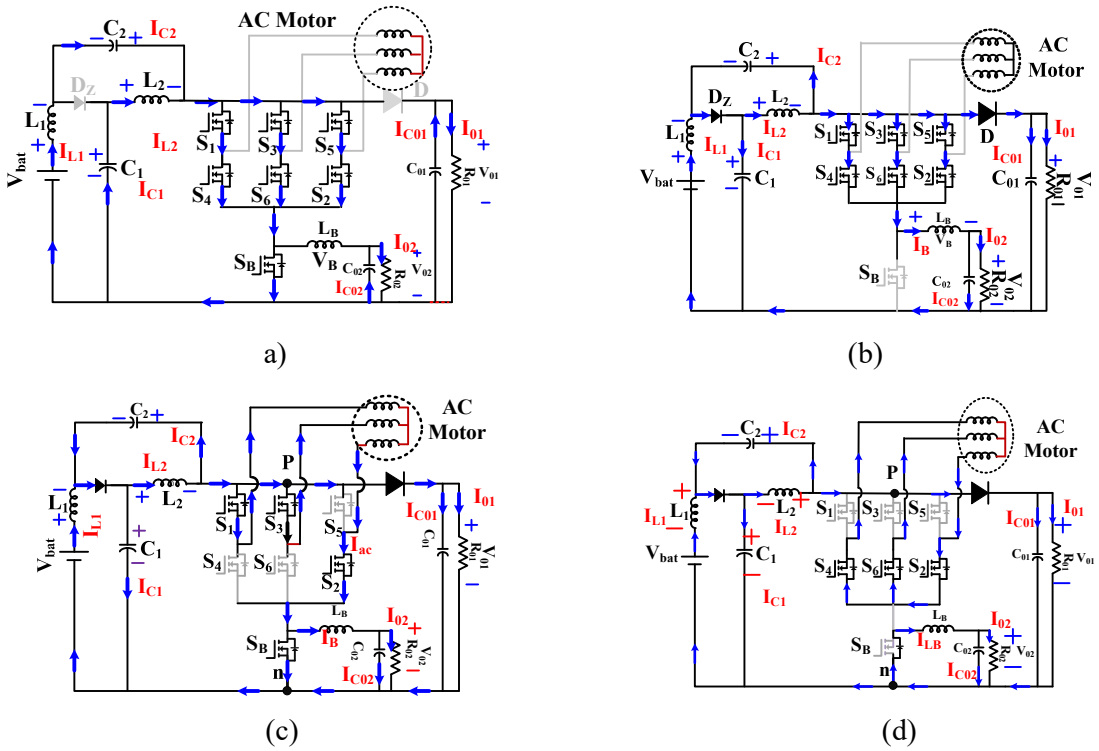

Fig.2. 8 (a) complete shoot-through operation, (b) inverter shoot-through operation, (c) power stage of the non-shoot-through interval, and (d) zero state of the non-shoot-through interval of the PPP.

1) three-phase buck-boost AC output for driving the AC motor, 2) and 3) two separate DC outputs of V_{01} and V_{02}, to power support the EV cabin.

2.2.1.3 Motoring mode operation with inherent Q-ZSI-based circuit:

a) Interval I- Complete shoot-through operation (D_1T_S):

The operation of the Q-ZSI-based circuit in a complete shoot-through interval is shown in Fig.2. 8 (a). During interval I, the complete shoot-through operation is performed, where all the switches are turned ON, along with the switch S_B. For dividing the current stress, three legs of the inverter have been chosen for the inverter shoot-through operation.

The governing equations during this interval are written as follows:

$$v_{L1} = v_{bat} + v_{C2}, v_{L2} = v_{C1}; v_B = -v_{02}, i_{C1} = -i_{L2}; i_{C2} = -i_{L1}, i_{Co} = -i_{01},$$

$$i_{C02} = i_B - i_{02}.$$

b) Interval II- Inverter shoot-through operation (D_2T_S):

In inverter shoot-through operation, switch S_B is turned off, compared to the complete shoot-through interval. The circuit schematic under this interval is shown in Fig.2. 8 (b).

The equations of the converter during this interval are as follows. $v_{L1} = v_{bat} - v_{c1}$,$v_{L2} = -v_{C2} = v_{C1} - v_{01}$, $v_{LB} = v_{C1} + v_{C2} - v_{02} = v_{01} - v_{02}$, $i_{C2} + i_{C01} + i_{Lb} = i_{L2} - i_{01}$,$i_{C02} = i_{Lb} - i_{02}$, and $i_{C1} = i_{L1} - i_{Lb} - i_{C01} - i_{01}$.

c) Interval III- Non-shoot through state (D_3T_S):

This interval is divided into two sub-intervals: a) power state and b) zero state. The equivalent circuit diagrams during power and zero states are shown in Fig.2. 8 (c) and (d). In the power state, one of the three cases is possible: 1) the upper switch of one leg and the lower switch from one of the other two legs are ON, 2) the upper switch of one leg and lower switch of the other two legs are ON, 3) two switches of the upper leg and one switch of the other legs are ON. The state of the switching can be selected according to the motor used in the EV. Further, in zero states, either all three high-side switches (S_1, S_3, S_5) or all three low-side switches (S_4, S_6, S_2) are turned OFF simultaneously.

The equations during this interval are as follows: $v_{L1} = v_{bat} - v_{C1}$, $v_{L2} = -v_{C2} = v_{C1} - v_{01}$, $v_B = -v_{02}$; $v_{PN} = v_{01}$,$i_{c2} = i_{L2} - i_{01} - i_{C01} - i_{ac}$,$i_{C1} = i_{L1} - i_{C01} - i_{ac} - i_{01}$; and $i_{C02} = i_B - i_{02}$. T_S is the total time period.

i) Steady State Analysis in motoring mode:

For the proper operation of the converter, the following conditions must be satisfied:

$$M_a+D_1+D_2=1 \tag{2.5}$$

where M_a is the modulation index, D_1 is the duty ratio of the complete shoot-through operation, and D_2 is the duty ratio of the only inverter shoots-through operation.

By applying volt-sec balance and charge–sec balance, the steady state relations are obtained as

$$V_{01} = \frac{V_{bat}}{1-2D_1} \tag{2.6}$$

$$V_{02} = \frac{V_{bat}*D_2}{1-2D_1} \tag{2.7}$$

For a three-phase induction motor,

$$\text{AC peak } V_{ac\_pk} = \frac{V_{bat}*M_a}{(1-2D_1)} \tag{2.8}$$

2.2.2 Multimode property of the PPP

2.2.2.1 V2V charging operation of the PPP

For V2V charging, additional switches N3, N4, N5, and N6's CM-NO are connected in PPP for the energy exchange between the energy supplier and the energy acceptor vehicle, as shown

in Fig.2. 5. The energy supplier vehicle circuit is shown in Fig.2. *5*(a), and the energy acceptor vehicle is shown in Fig.2. 5(b). The high-power auxiliary terminal V_{01} is selected for the connecting point for this energy exchange. The cabin power of the energy supplier vehicle is unaffected during this operation, while only the high-power auxiliary is powered in the energy acceptor vehicle.

2.3 Design of the Circuit Parameters:

The PPP operates in both multifunctional and multimode configurations, making circuit parameters critical to its overall design. For its healthy operation, component ratings are calculated in both multifunction and multimode operations, and higher rating components are selected for their effective operation.

2.3.1 Elements of the power factor correction circuit of PPP:

The rating of the boost inductor is determined by the maximum inductor current ripple to ensure that the converter operates in continuous conduction mode. The value of the inductor is calculated using the formula given in Error! Reference source not found. (a).

where: V_{ac} is RMS input voltage; $\%I_{ripple}$ is the percentage of inductor ripple current regulation; P_o is maximum steady state power; f_{sw} is switching frequency; V_{DC} is DC-link voltage.

The rating of the DC-link capacitor is determined by either hold-up time or voltage ripple limitation. Its value is typically taken as one cycle (10ms in this case). The greater value of the capacitor should be considered from the given equations in Table 2. 2(b).

where: t_{hold} is hold-up time, V_{min} is the minimum voltage to which the output voltage is allowed to drop, f_{line} is the input line frequency, and ΔV_o is the specified voltage ripple.

2.3.2 Elements for intermediate DC-DC and the multioutput during charging mode:

Three outputs are generated in the multioutput operation. In charging mode, the intermediate DC-DC converter charges the battery, and dual outputs are generated along with that. The element rating for the intermediate DC-DC converter is given in Table 2. 2, (d), and the component rating for the dual outputs are given in Table 2. 2, (e)-(h).

2.3.3 Rating of the components for motoring operation:

In the inverter network, two inductors and two capacitors are used to absorb the current and voltage ripple. For a complete shoot-through interval, $dt=D_1T_S$, the inductor current ripple is $di_L = \Delta i_L$. So, the value of the inductor will be calculated from Table 2. 2, (a)-(c).

For the complete shoot-through interval, dt =D_1T_s, the voltage ripple in the capacitor is $dv_C = \Delta v_c$. Using this, the value of capacitors will be given as:

$$C = C_1 = C_2 = \frac{I_L * D_1}{\Delta v_c * f_s} \tag{2.9}$$

2.3.4 Rating of the components for V2V charging:

L_A and L_B inductances are determined by the maximum current ripple limit during complete shoot-through and power state for the multioutput operation. So, the value of the inductor will be calculated from Table 2. 2 e-f.

$$L_A = \frac{V_{bat} * D1}{f_s * \Delta I_A} \tag{2.10}$$

$$L_B = \frac{(V_{bat} - V_{02}) * D_2}{f_s * \Delta I_B} \tag{2.11}$$

Table 2. 2 Rating of the selected components

	Charging mode	Propulsion Mode	Components
(a)	$L_1 + L_2 = \frac{{V_{ac}}^2}{\%I_{ripple} * P_o * f_{sw}}\left(1 - \frac{\sqrt{2} * V_{ac}}{V_{DC}}\right)$	$L_1 = L_2 = \frac{V_{bat} * (1 - D_1) * D_1}{(1 - 2D_1) * \Delta i_L * f_s}$	1mH
(b)	$C_{dc\_link} \geq \frac{2 * P_o * t_{hold}}{{V_o}^2 - {V_{min}}^2}, C_{dc\_link} \geq \frac{P_o}{2 * \pi * f_{line} * \Delta V_o * V_o}$	According to filter	3mF
(c)	Not required	$C_1 = C_2 = \frac{I_L * D_1}{\Delta v_c * f_s}$	564µF
(d)	L_r and C_r are selected according to the resonance frequency	Not required	32µH, 2 µF
(e)	$L_A = \frac{V_{Bat} * D1}{f_s * R_{01} * \%\ ripple\ allow\ I_{01}}$	Not required	0.8mH
(f)	$L_B = \frac{(V_{01} - V_{02}) * D_2)}{f_s * \%\ ripple\ allow\ I_{02}}$	$L_B = \frac{(V_{01} - V_{02}) * D_2)}{f_s * \%\ ripple\ allow\ I_{02}}$	0.8mH
(g)	$C_{01} = \frac{V_{Bat} * D1}{f_s * R_{01} * \%\ ripple\ allow\ V_{01}}$	$C_{01} = \frac{V_{Bat} * D1}{f_s * R_{01} * \%\ ripple\ allow\ V_{01}}$	470µF
(h)	$C_{02} = \frac{V_{Bat} * (1 - D1 - D_2) * D_2}{8 * {f_s}^2 * (1 - D_1) * \%\ ripple\ allow\ V_{02} * L_B}$	$C_{02} = \frac{V_{Bat} * (1 - D1 - D_2) * D_2}{8 * {f_s}^2 * (1 - D_1) * \%\ ripple\ allow\ V_{02} * L_B}$	100µF

2.3.5 Selection of the components in the proposed power processor:

The higher rating from $(L_1 + L_2)/2$ is selected for L_1 and L_2. The C_1 and C_2 value is selected from a higher value in between them. The DC-link capacitor value during charging

mode is selected to be a higher value than the $C_{dc\text{-}link1}$ and $C_{dc\text{-}link2}$. The intermediate DC-DC components are selected from the converter's series resonance condition. First, select the nominal frequency where the switching frequency is equal to the resonant frequency. Then, the value of the inductor is selected according to the ripple minimization and current healing capacity of the wire used in the inductor winding. After that, the capacitor is selected according to the nominal frequency. The components rating for the PPP operation is shown in Table 2. 2.

2.4 Dynamic analysis and M-SPWM scheme:

The control scheme of multifunction and multimode operation of the proposed power processor are explained in this section.

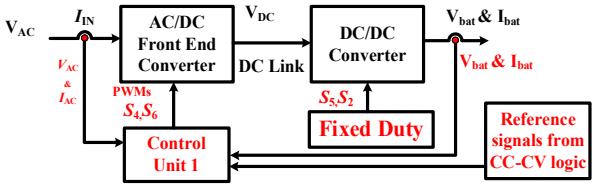

Fig.2. 9 Control logic block diagram of battery charging.

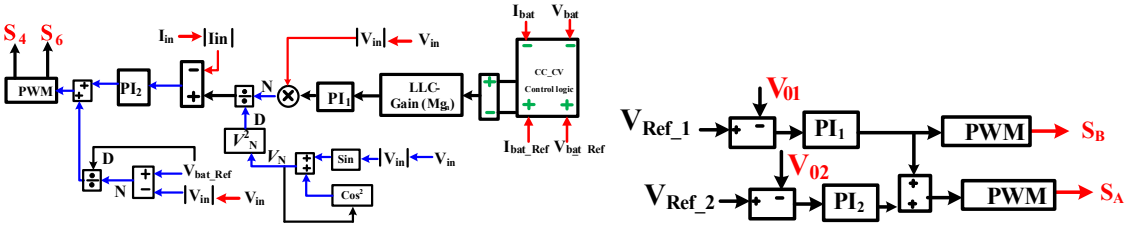

(a) (b)

Fig.2. 10 The control logic of charging mode: (a) control unit I maintains the unity power factor at the source terminal and charges the battery with CC-CV charging, (b) control unit II regulates the multioutputs for the auxiliary power supply.

2.4.1 Control scheme for the charging mode:

The important parts of the proposed algorithm are to get power factor correction (PFC) and regulate the battery voltage and current by using cascaded loops, as shown in Fig.2. 9. This is unlike the conventional approach, in which two separate controllers are used to get PFC and regulate battery voltage and current. The existing control loop structure of PFC with multioutputs of the PPP is given in Fig.2. 10.

2.4.1.1 Implementation of the constant-current constant-voltage (CC-CV) charging technique:

The battery is charged through the CC-CV charging technique for its long life [92], [93]. In this charging technique, the battery's 80 to 90 percent State of Charge (SOC) is charged through the CC method, and the remaining SOC of the battery is charged through the CV method [94], [95]. The set battery voltage is taken as a reference where the SOC is not available.

2.4.1.2 Control technique for intermediate DC-DC converter:

The intermediate DC-DC converter provides the constant gain by switching the switches S_5 and S_2 at the normalized frequency ($f_n = \frac{f_{switchin}}{f_{resonance}}$) with a fixed duty ratio. It simplified the conventional control scheme of two separate controllers for AC/DC and DC/DC converters, as shown in Fig.2. 9.

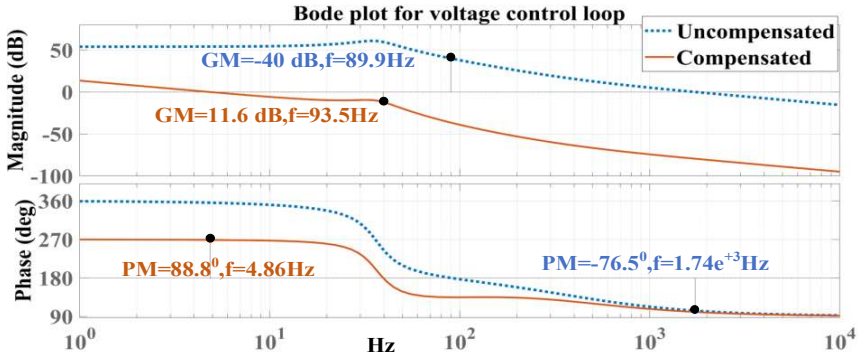

(a)

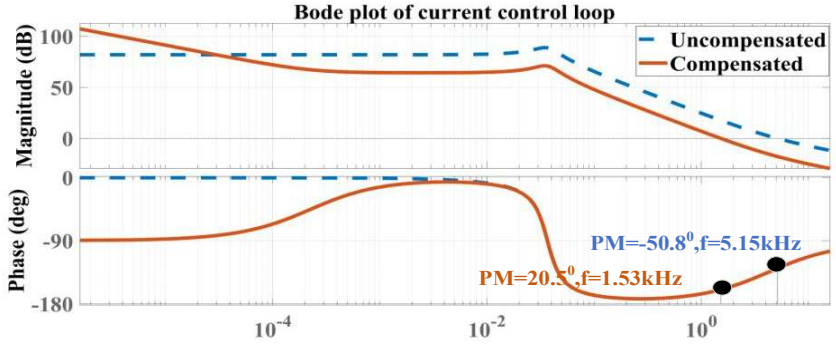

(b)

Fig.2. 11 Bode plot, (a) voltage control loop, and (b) current control loop.

2.4.1.3 PI controllers in the charging mode:

A cascaded loop has been used to obtain the CC or CV reference and unity power factor (UPF). The PI_1 controller is used to set the desired current or voltage for CC and CV charging, and the PI_2 controller is used to maintain the PFC at the input terminal.

The PI_1 controller value is obtained by the small signal analysis of the converter, which determines the voltage loop transfer function of $\frac{\hat{v}_{bat}}{\hat{\imath}_{in}}$. To minimize the effect of the low-order harmonics on input current, THD, and for the stability of the converter, the outer voltage loop compensator (PI_1) should be designed to have a narrow bandwidth. Here, it is kept around 4.86 Hz, as shown in Fig.2. 11(a). The bandwidth of the inner current control loop (PI_2) should be below 1/10th of the switching frequency [96]. The value of the PI_2 controller is determined by the current loop transfer function of $\frac{\hat{\imath}_{in}}{\hat{D}}$. It is kept around 1.53 kHz, as shown in Fig.2. 11(b). The duty ratio $\widehat{D}$ generates the PWM for switches S_4 and S_6 to achieve the desired value of current or voltage and maintains the unity power factor at the source terminal.

2.4.1.4 Control technique for the multioutput:

The control structure of the multioutput is shown in Fig.2. 10(b). It maintains the desired values for the power support of the EV cabin in charging mode. In the motoring mode, the same value is maintained by the fixed duty ratio of D_1 and D_2 with the modified control schemes. The control parameter for PI_1 is determined by the V_{01}/D_1 transfer function, and the control parameter for PI_2 is determined by the V_{02}/D_2 transfer function. Where D_1 is the complete shoot-through duty ratio D_1 (S_A and S_B are ON), and D_2 is the power state duty ratio (S_A ON and S_B OFF).

Further, in propulsion mode, V_{01} is controlled by the Eq. 2.6 complete complete-through duty ratio D_1 (all switches of the inverter S1, S_2, S_3, S_4, S_5, S_6, and S_B are ON), and V02 is controlled by the Eq. 2.7 inverter shoot-through duty ratio D_2 (all switches of the inverter S1, S_2, S_3, S_4, S_5, S_6, ON and S_B OFF) by fixing the duty ratio D_1.

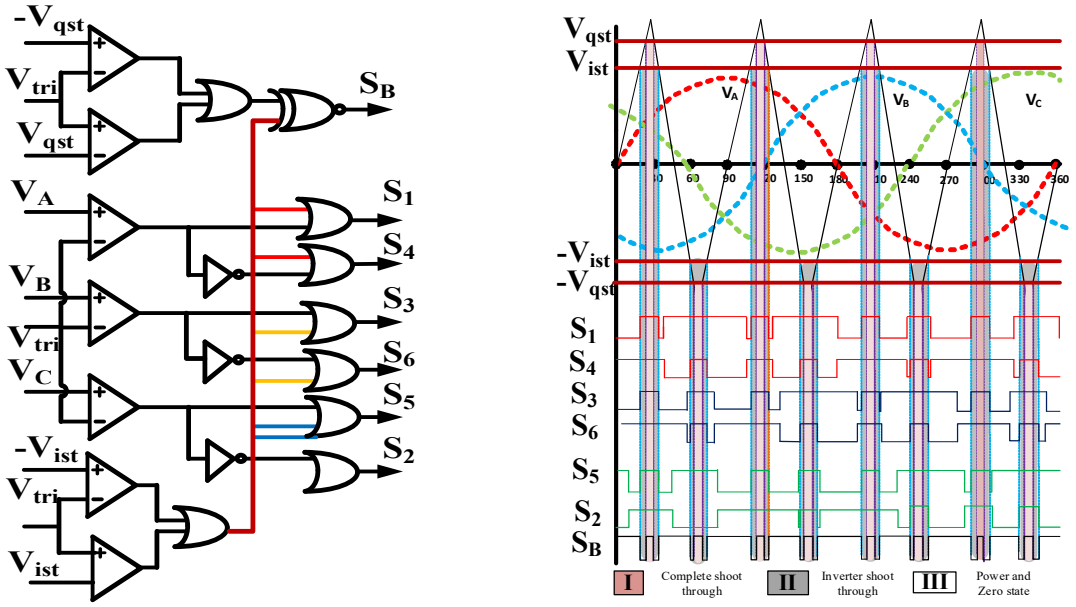

(a) (b)

Fig.2. 12 (a) Pulse generation logic for modified SPWM, and (b) generated switching signals for modified SPWM.

2.4.2 Control scheme for motoring mode:

The control logic for the proposed power processor to drive the AC motor during propulsion operation is shown in Fig.2. 12 (a). The expressions of these reference signals are as follows:

$V_{qst} = \hat{V}_{tri}(1 - D_1)$,$V_{ist} = \hat{V}_{tri}(1 - D_1 - D_2)$, $V_A = \hat{V}_{tri} * M_a sin(wt)$, $V_B = \hat{V}_{tri} * M_a sin(wt - 120^o)$, and $V_C = \hat{V}_{tri} * M_a sin(wt + 120^o)$.

From the above equations, it can be concluded that the V_{01} is controlled by the complete shoot-through duty ratio (D_1), the V_{02} is controlled by the inverter shoot-through duty ratio (D_2) by fixing the D_1, and the inverter output voltage is controlled by the modulation index (Ma=1-D_1-D_2), by fixing the D_1 and D_2.

The PWM waveforms for the modified simple boost-control scheme are shown in Fig.2. 12(b). Interval I, represents the complete shoot-through, interval II represents the inverter shoot-through, and interval III represents the power and zero state. The zero states of the conventional voltage source inverter (VSI) are utilized as a complete shoot-through, and an inverter shoot-through interval to boost the AC output voltage.

Table 2. 3 Design specification of the proposed converter

Specifications	Values	Specifications	Values
V_{bat}	48 V	f_{S_Motor}	20 kHz
V_{01}	72 V	D_{1_Motor}	0.125
V_{02}	12 V	D_{2_Motor}	0.25
V_{ac_out}	30 V	M_a	0.625
Power	550 W	f_{S_LLC}	19.99 k Hz
$f_{S\_Boost\ PFC}$	20 kHz	$f_{S\_Multioutput}$	20 kHz

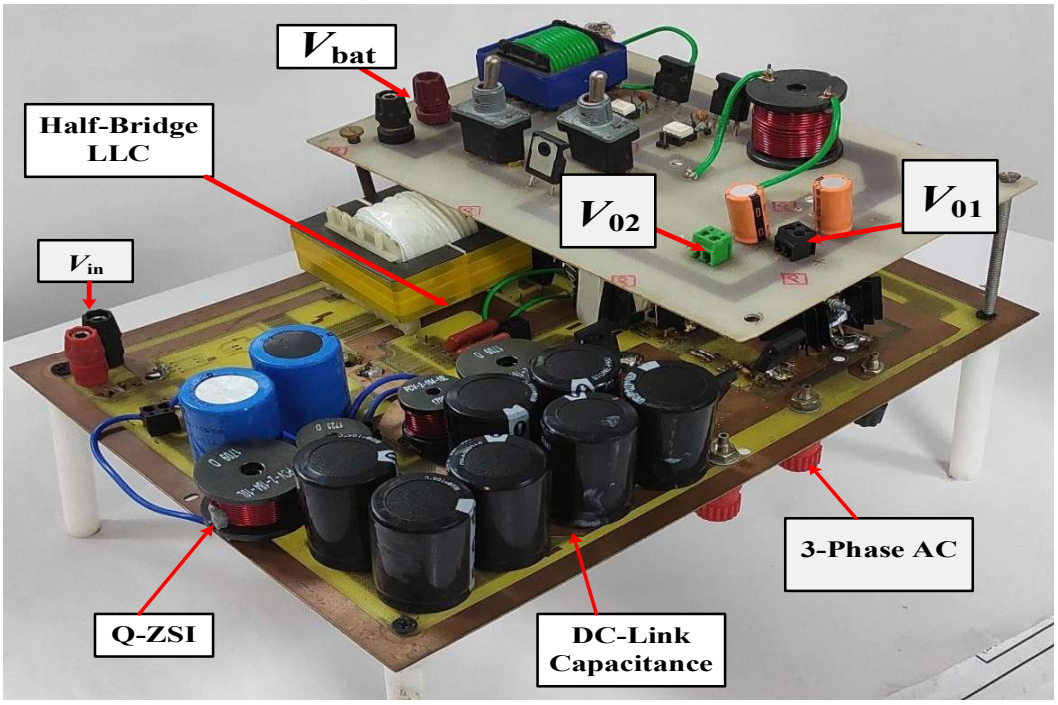

Fig.2. 13 Photograph of the proposed power processor.

2.5 Experimental validation

The specification of the proposed power processor is given in Table 2. 3. The photograph of the experimental prototype is shown in Fig.2. 13. For better understanding, the experimental results are divided into two sections: multifunction and multimode operation of the proposed power processor, i.e., a) 1-Φ on-board charging mode, and propulsion mode. b) V2V charging operation.

2.5.1 Charging mode operation:

2.5.1.1 PFC with CC-CV charging:

In charging mode, three outputs are generated from the single-phase AC supply of 120V, 50 Hz. The first output charges the battery with CC-CV charging, and the second and third

outputs supply power to the EV cabin. The unity power factor at the source terminal with multioutputs is shown in Fig.2. 14(a). V_{01}, V_{AC}, and V_{02} are the boost multioutput voltage, AC input voltage, buck multioutput voltage, and I_{AC} is the input AC current. The CC-CV charging is tested by the resistive load, as shown in Fig.2. 14(b). The transition point is set to 51 V; therefore, till 51 V, the battery is charged through 5 A of current. After that, the current decreases, and the voltage increases.

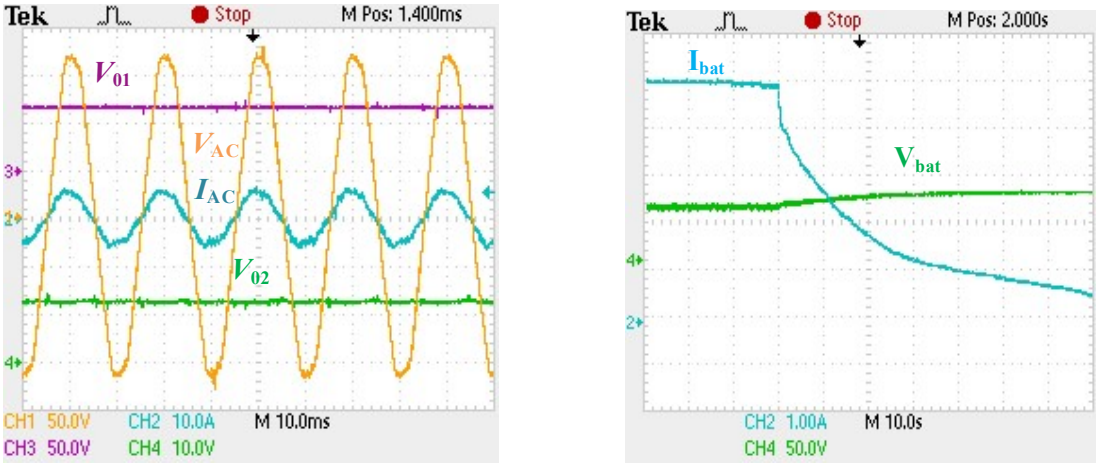

(a) (b)

Fig.2. 14 In charging mode, (a) unity power factor with multioutputs, (b) CC-CV charging.

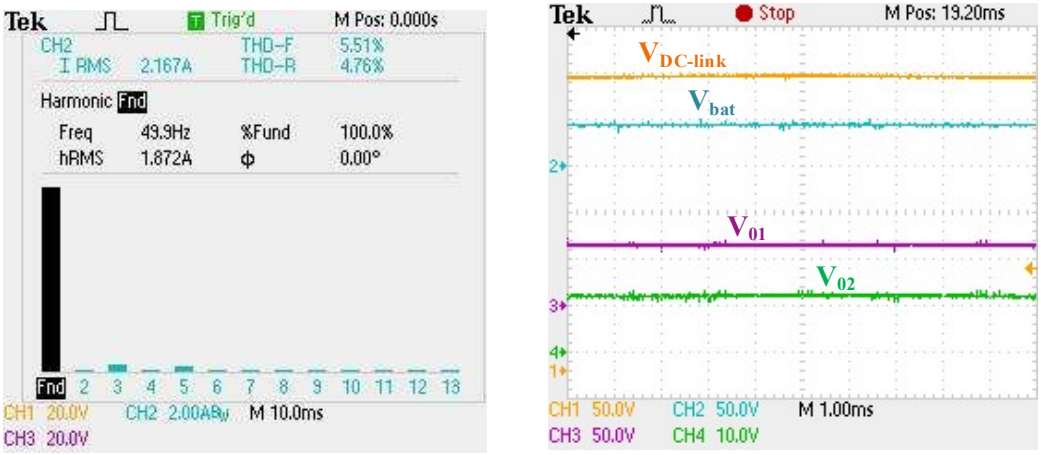

(a) (b)

Fig.2. 15 In charging, (a) THD spectrum of source current, and (b) the available output voltages.

2.5.1.2 THD spectrum of source current and multioutput:

The THD spectrum of the source current is given in Fig.2. 15 (a), and the available outputs during charging mode are shown in Fig.2. 15(b). $V_{DC\text{-}link}$, V_{bat}, V_{01}, and V_{02} are the DC-link

voltage, battery voltage, boost output voltage for high-power auxiliaries, and the buck voltage for low-power auxiliaries.

2.5.1.3 ZVS of the intermediate DC-DC converter and switching for the multioutput:

For the ZVS condition, when the switch is turned on, the voltage drop at the switch is zero, and at that time, the current should be lagging. Furthermore, the series resonance current flow through the circuit should be sinusoidal. The ZVS of the intermediate DC-DC converter is shown in Fig.2. 16(a). The converter's operation during multi-output mode is illustrated in Fig.2. 16(b). In this figure, $\mathbf{I_{LA}}$ and $\mathbf{I_{LB}}$ denote the charging and discharging currents of inductors $\mathbf{L_A}$ and $\mathbf{L_B}$, respectively, corresponding to the switching actions of $\mathbf{S_A}$ and $\mathbf{S_B}$. Additionally, $\mathbf{V_{A\_DS}}$ and $\mathbf{V_{B\_DS}}$ represent the voltages across switches $\mathbf{S_A}$ and $\mathbf{S_B}$.

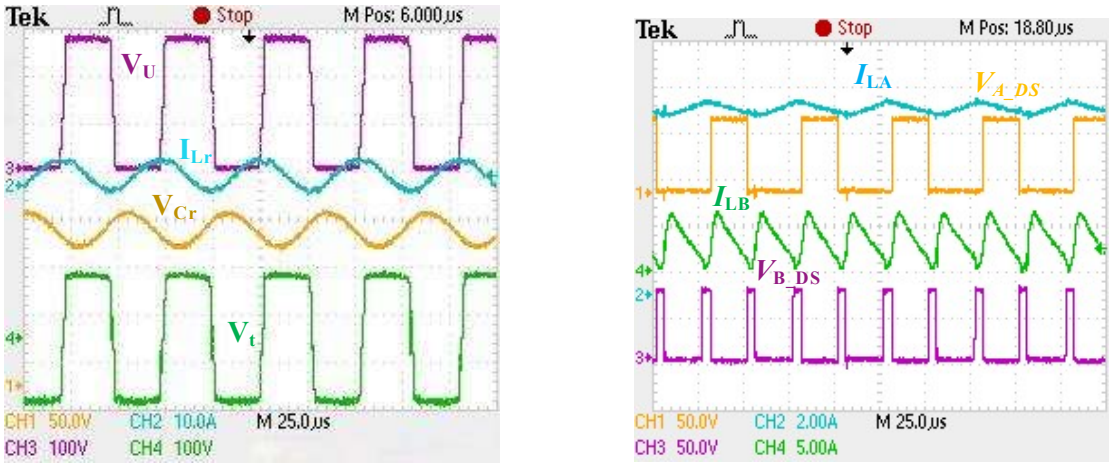

(a) (b)

Fig.2. 16 In charging, (a) zero voltage switching with series resonance operation of the intermediate part of the PPP, and (b) voltage drop across switches S_A and SB, with the inductor LA and LB current profile during multi-output operation.

2.5.2 Motoring operation of the proposed power processor:

The operation of the PPP in propulsion mode can be understood by the switching sequence and the output obtained by that switching. The switching sequence of the PPP in propulsion mode is shown in Fig.2. 17 (a) and (b). It is divided into three intervals 1) complete shoot-through, 2) inverter shoot-through, and 3) power and zero state of the converter. In the complete shoot-through interval, all the inverter switches $\boldsymbol{S_1}, \boldsymbol{S_2}, \boldsymbol{S_3}, \boldsymbol{S_4}, \boldsymbol{S_5}, \boldsymbol{S_6}$, and the switch $\boldsymbol{S_B}$ are turned ON. Further, in the inverter shoot-through interval, only the switch S_B is turned off compared

to the complete shoot-through. The switching states are changes in the zero state just before and after the complete shoot-though intervals; that's why the switching losses are reduced.

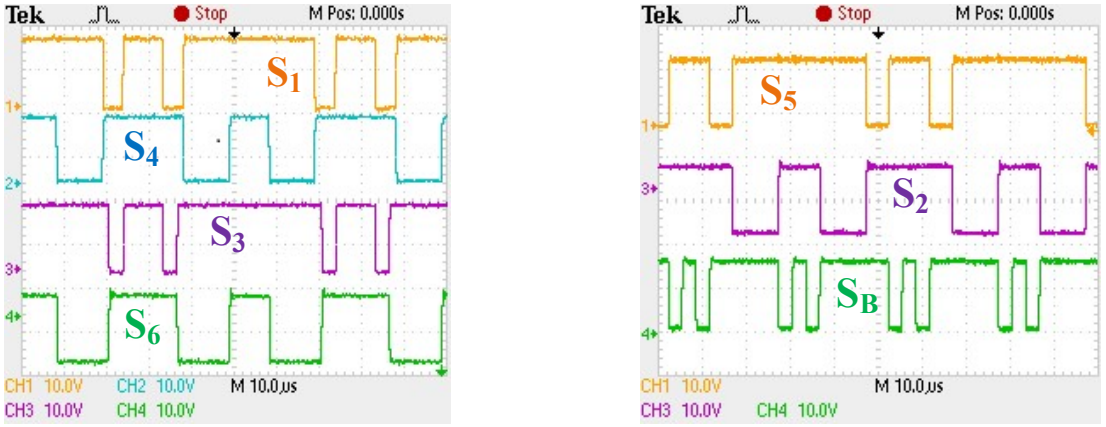

(a) (b)

Fig.2. 17 Switching sequence S_1, S_4, S_3, S_6, and S_5, S_2, S_B of the proposed power processor during propulsion mode.

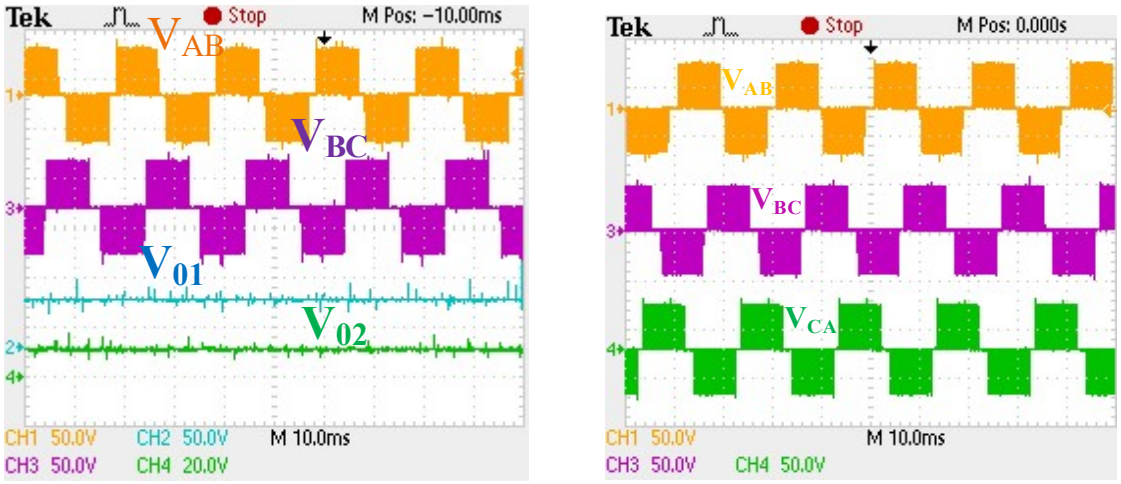

(a) (b)

Fig.2. 18 (a) Inverter line voltage V_{AB} and V_{BC} with multioutput voltages V_{01} and V_{02}, and (b) Inverter line voltages V_{AB}, V_{BC}, and V_{CA} are 120^0 phase-shifted from each other.

The ppp generates three outputs from the battery: 1) buck-boost AC, which can drive the Low-power AC motor, 2) V_{01}(boost), and 3) V_{02}(buck) voltages support the low and high-power auxiliaries of the EV cabin, as shown in Fig.2. 18(a). The boost line voltages $\mathbf{V_{AB}}$, $\mathbf{V_{BC}}$, and $\mathbf{V_{CA}}$ are 120^o apart from each other, as shown in Fig.2. 18(b).

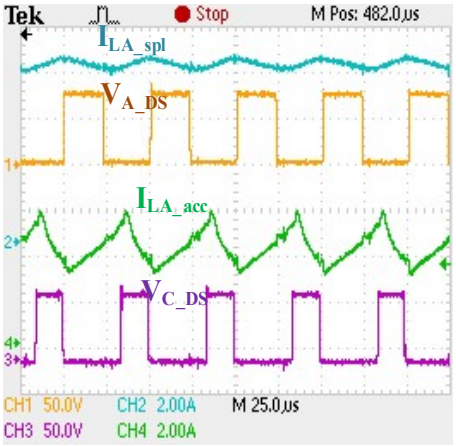

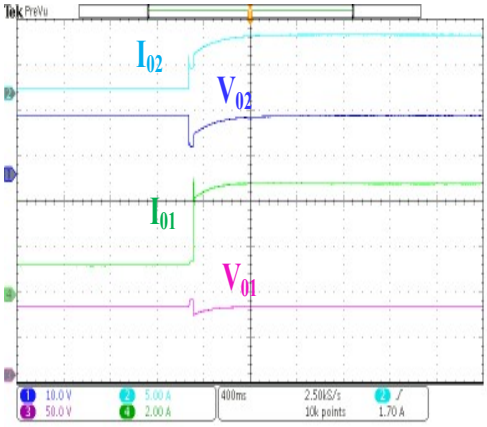

(a) (b)

Fig.2. 19 (a) switching for the V2V energy transfer with inductor energy balancing, (b) load dynamics during V2V charging.

2.5.3 V2V charging during multimode operation:

p. In Fig.2. 19(a), $\mathbf{I_{LA\_spl}}$ and $\mathbf{I_{LA\text{-}acc}}$ show the charging and discharging currents of the energy supplier and the energy acceptor vehicle inductor $\mathbf{L_{A\text{-}spl}}$, and $\mathbf{L_{A\text{-}acc}}$, respectively, corresponding to the switching action of S_A and S_C. $\mathbf{V_{A\text{-}DS}}$ and $\mathbf{V_{C\text{-}DS}}$ represent the voltage across the switches S_A and S_C during the V2V operation. During V2V charging operation, the resistive load dynamic is simultaneously applied in the high-power and low-power auxiliary. The stable voltage regulation is achieved within a short period of time, as shown in Fig.2. 19 (b). V_{01}, I_{01}, and V_{02}, I_{02} represent high-power auxiliary voltage and current and low-power auxiliary voltage and current, respectively.

2.6 Conclusion

This chapter presents a multifunction quasi-Z source-based multimode power processor for low-power EVs. In its multifunction operation, it charges the battery from the single-phase power supply and can drive the low-power 3-phase motor. Further, its multimode property is utilized for V2V charging and cabin auxiliary supply. In the charging operation, it charges the battery with either a 1-Φ phase AC supply or a DC (V2V) source and also generates the multioutputs. During 1-Φ phase AC charging, it maintains the unity power factor at the source terminal and protects the grid from harmonic pollution. Also, it generates three outputs, 48 V,12 V, and 72 V, from the 120 V 50 Hz household power supply. 48 V outputs charge the battery with the CC-CV charging technique, and 12 V and 72 V supply power to the EV cabin. In V2V charging, four changeover switches are used to form the circuit of energy supplier and acceptor vehicles for energy exchange. In motoring mode, three outputs are generated from the proposed

modified boost sinusoidal pulse width modulation (M-SPWM). It generates buck-boost AC, which can drive the AC motor, and 12 V and 72 V cater to the power demand of the EV cabin from the 48 V battery. The 12 V generated output eliminates the 12 V battery and its charger, and the 72 V generated output provides the selection of high-power auxiliaries other than the battery voltage. For the validation, the theoretical concept is implemented in 550 W of a laboratory-scale prototype.

The work carried out in this chapter has some limitations: 1) The application of the proposed power processor is limited, and it can fit in the application of 36 V, golf cart EVs like (Club car, E-Z-GO, etc.), and 2) Four switches are used to form the energy supplier and acceptor vehicles circuit for the energy exchange.

In the next chapter, the previously identified limitations are addressed through the design of an improved version of the power processor. To address these challenges, the integrated circuit is further developed to drive a 48 V Brushless DC (BLDC) motor using the High-PWM Low-ON (HPLN) switching technique, which is particularly suited for applications such as electric rickshaws and light electric utility vehicles. The HPLN switching significantly reduces commutation torque ripple during motoring operation, thereby enhancing motor performance. Three changeover switches are used to form the circuit of the energy supplier and the acceptor vehicle for V2V charging. Furthermore, a comprehensive cost analysis and evaluation of the converter's power density are carried out, offering valuable insights into the economic viability of the proposed system